Sugarcane image stitching under transverse transport based on improved SURF algorithm

Deqiang Zhou[1*], Jiahao Zhu[1], Wenbo Zhao[1], Fengguang He[2], Lijiao Wei[2], Ganran Deng[2]
(1. *School of Intelligent Manufacturing, Jiangnan University, Wuxi 214401, China*;
2. *Agro-Machinery Research Institute, Chinese Academy of Tropical Agricultural Sciences, Zhanjiang 524000, China*)

Abstract: This paper proposes a sugarcane image stitching algorithm based on an improved SURF method to capture high-quality, wide-field images of complete sugarcane stalks. To enhance registration accuracy, artificial markers are introduced into the background, helping to address the challenges posed by the smooth surface of sugarcane and low feature point matching precision. Additionally, a mesh segmentation technique combined with an enhanced SURF algorithm is used for feature extraction, which tackles issues such as uneven feature distribution and slow processing speed caused by global image feature extraction. A double screening registration method is also proposed to further improve the accuracy of image mosaicing. To reduce stitching gaps, an image fusion technique based on the optimal suture line is employed. Experimental results show that the algorithm has an average runtime of about 2900 ms, slightly longer than the ORB algorithm at 2000 ms but significantly faster than the original SURF at 4200 ms. In terms of stitching quality, the average image information entropy is 6.34, which is higher than both the SURF (6.325) and ORB (6.075) algorithms, indicating better image quality.
Keywords: sugarcane image, image stitching, image registration, feature extraction, feature matching, SURF
DOI: 10.25165/j.ijabe.20251805.9058

Citation: Zhou D Q, Zhu J H, Zhao W B, He F G, Wei L J, Deng G R. Sugarcane image stitching under transverse transport based on improved SURF algorithm. Int J Agric & Biol Eng, 2025; 18(5): 278–286.

1 Introduction

Sugarcane is a major sugar crop widely cultivated in tropical and subtropical regions, with China being one of its largest producers. Currently, sugarcane planting in China involves real-time cutting and pre-cutting methods. However, the complex and harsh working environment of agricultural machinery, coupled with various on-site environmental factors, pose challenges to the accurate and efficient sugarcane identification and cutting. In the field of sugarcane planting mechanization, the recognition algorithm plays a pivotal role for sugarcane inspection and cutting. It needs to quickly and accurately detect the sugarcane nodes in complex and dynamic working environments, as the speed and accuracy of recognition directly affect the performance of the cutting machine. Currently, there are several machine vision-based methods developed for this purpose. Some scholars[1-4] utilize manual feature extraction, such as gradients and colors, to recognize sugarcane stem nodes. However, these methods requires prior knowledge and a large number of parameters, resulting in poor robustness. More recently, references[5,6] use deep learning-based single-stage object detection algorithms, which improves the accuracy and efficiency of the sugarcane stem recognition to some extent. Despite these advancements, the relatively long overall size of sugarcane poses a unique challenge, as a single camera cannot capture the node information of the entire sugarcane due to insufficient field of view. This limitation necessitates segmented cutting, resulting in relatively low efficiency. To address the issue of insufficient field of view, image stitching[7] has become the mainstream method due to its unique advantages of enabling the acquisition of complete visual information through the assembly of multiple images captured from various perspectives. Image stitching process mainly includes image preprocessing, image registration, and fusion[8], with image registration being the most critical aspect. Based on different registration methods, image stitching methods can be divided into two types. One is region-based image stitching methods, which mainly uses pixel grayscale information to find similar template windows for matching, such as template matching[9], phase correlation[10], and extended phase correlation[11]. However, region-based image stitching methods have limited applicability and high computational complexity. The other type is feature-based image stitching, which is more efficient and robust, utilizing key point information in the images for matching exemplified by algorithms, such as the Harris corner detection[12], Scale-invariant Feature Transform (SIFT)[13], Speeded Up Robust Features (SURF)[14], etc.

Region-based image stitching methods are suitable for a limited number of scenarios and often involve a higher computational complexity and have become the predominant method for image stitching due to their effectiveness. Lee et al.[15] proposed a large-disparity image stitching algorithm based on warping residuals to address the parallax issue caused by images taken from different planes, which existing stitching algorithms fail to solve. Bouchekara et al.[16] addressed the issues of limited features and low resolution in drone images by proposing an object-based four-stage image stitching method, which overcomes the dependency on the quality of feature recognition in traditional stitching methods. Daniel et

Received date: 2024-05-12 **Accepted date:** 2025-07-11
Biographies: Jiahao Zhu, MS, research interest: smart agriculture, Email: 975602233@qq.com; **WenBo Zhao**, MS, research interest: smart agriculture, Email: 1475817953@qq.com; **Fengguang He**, Assistant Researcher, research interest: tropical agricultural machinery, Email: 879909560@qq.com; **Lijiao Wei**, Associate Researcher, research interest: tropical agricultural machinery, Email: 406775423@qq.com; **Ganran Deng**, Researcher, research interest: tropical agricultural machinery, Email: dengganran@163.com.
***Corresponding author: Deqiang Zhou**, Associate Professor, research interest: smart agriculture. School of Intelligent Manufacturing, Jiangnan University, Wuxi 214401, China, Tel: +86-18724042406, Email: zhoudeqiang@jiangnan.edu.cn.

al.[17] introduced and evaluated four new global image stitching algorithms, achieving the fusion of high-noise and low-contrast SEM images. Chen et al.[18] proposed a drone image stitching method based on an optimal seam blending algorithm and semi-projection transformation to eliminate deformation and angle distortion caused by image registration. This method effectively preserves the original information of the images and achieves the desired stitching effect. Subramanyam et al.[19] proposed a hybrid descriptor that effectively stitches multiple camera-captured ground texture images using defect detection. This method outperforms existing feature descriptors in terms of matching accuracy, achieving a matching accuracy of 91% with an execution time of 49 milliseconds, enabling seamless stitching. Li et al.[20] proposed a pre-alignment image stitching method for a scanning imaging system based on Risley prisms. This method reduces the computational complexity of feature extraction and image registration. Huang et al.[21] constructed a novel convolutional network called DPH-Net, which incorporates depth information and pixel-level homography estimation into image registration for image matching. Based on the analysis above, image stitching is a promising method to effectively obtain high-quality images of large objects that cannot be captured within the limited field of view of a regular industrial camera. Considering stitching quality and speed, in the case of the sugarcane recognition and cutting system, this study focuses on refining stitching methods to obtain high-quality, wide-field-of-view images of complete sugarcane stalks.

2 Materials and methods

2.1 Image acquisition and preprocessing

To improve the image resolution while minimizing the hardware demands, we employed the Mercury series MER-531-20GC-P camera from Daheng Imaging Co. Ltd., equipped with an HN-0826-20M-C1/X1 fixed-focus lens. A camera polarizing filter (CPL) was added to the lens to eliminate glare and improve image quality. Two LS200F-HW line scan LED light source from Daheng Imaging were installed on both sides above the sugarcane, parallel to the axis of the sugarcane. Figures 1 and 2 illustrate the schematic and actual setup of our dual-camera sugarcane image acquisition system.

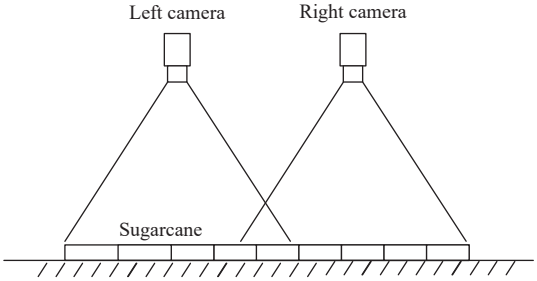

Figure 1 Schematic diagram of the dual-camera image acquisition solution

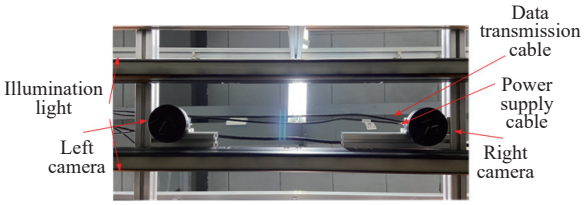

Figure 2 Actual setup of the dual-camera image acquisition system

Due to the smooth surface and the presence of wax powder on the sugarcane[22], it is prone to produce glare under the illumination of the light source. We mitigated this effect with the polarizing filter. The contrast of the images captured before and after installing the polarizing filter is shown in Figure 3. Artificial markers were addedtothebackground[23],enhancingtheregistrationaccuracybyproviding high-contrast feature points for the SURF algorithm to detect.

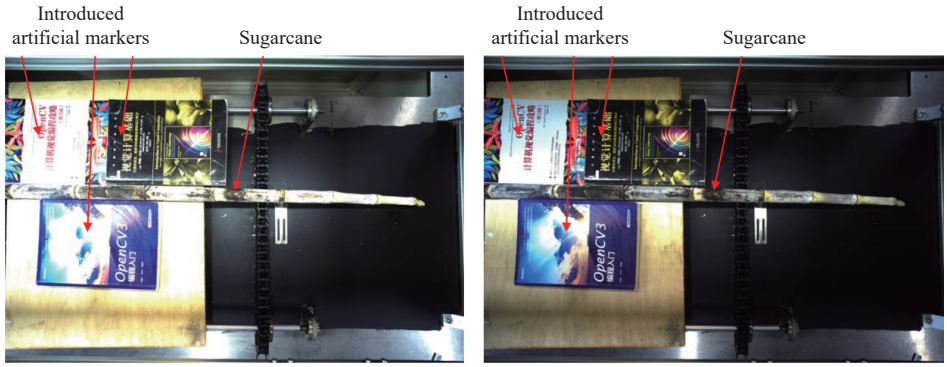

a. Before b. After

Figure 3 Comparison images before and after installing the polarizing filter

Meanwhile, filtering can effectively remove noise generated from different sources[18], resample the entire image, and extract meaningful feature information. In image processing, median filtering can effectively suppress random noise while preserving image edge information. It mainly applies the theory of order statistics to denoise the image. The process is shown in Formula (1):

$$Y(i,j) = \text{Median}(X(i,j)) \quad (i,j) \in A \tag{1}$$

where, $X(i,j)$ refers to pixel values of the points in the template window; A refers to the fixed-size template window; and Median() is a median function which returns the median pixel value of all points within the template window.

The variation in window size during the median filtering process significantly affects the filtering results. The window size is selected through experiments.

2.2 Feature point extraction and descriptors

2.2.1 Feature extraction

1) SURF

The SURF algorithm is derived from the Scale Invariant Feature Transform (SIFT) algorithm, with the main difference that the SURF introduces the concepts of integral images and box filters, greatly reducing the computational time. The key steps of the SURF

algorithm are shown in Figure 4.

The SIFT algorithm detects feature points by constructing a Gaussian difference pyramid, which is a computationally intensive and time-consuming process. In contrast, the SURF algorithm introduces the concept of integral images and box filters. It processes the input image using three types of box filters to obtain an approximation of the Hessian determinant. To ensure good rotational invariance of the selected feature points, the main orientation of each feature point needs to be determined. Unlike SIFT, which uses gradient histograms to determine the main orientation, SURF calculates Haar wavelet features within a neighborhood of radius 6 s (where s is the scale of the feature point) around the feature point to determine the main orientation, as shown in Figure 5. The horizontal and vertical Haar wavelet feature sums are computed in sector regions at intervals of 60°, and the sector with the highest sum determines the main orientation.

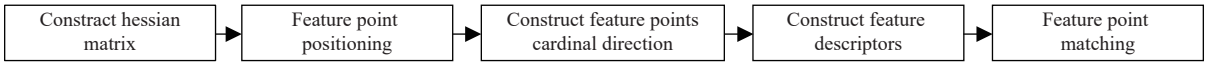

Figure 4 Key steps of the SURF algorithm

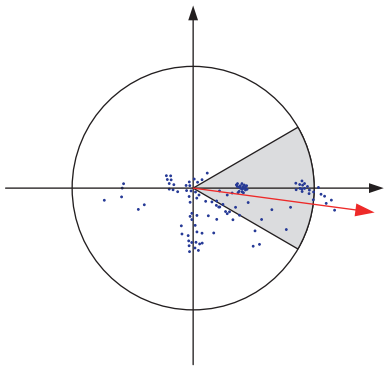

Figure 5 Main orientation of feature points

After completing the aforementioned steps, it is necessary to generate descriptors for the feature points for subsequent registration tasks. Based on the main orientation of the feature points, a region with a side length of 20 s (where s is the scale of the feature point) is selected in the vicinity of each feature point. Within this region, the absolute values and orientations of the Haar wavelet features are computed in 16 sub-regions. These results are in a total of 16×4=64 parameters, as shown in Figure 6. Compared to SIFT's 128-dimensional descriptor vector, the number of parameters in SURF is significantly reduced.

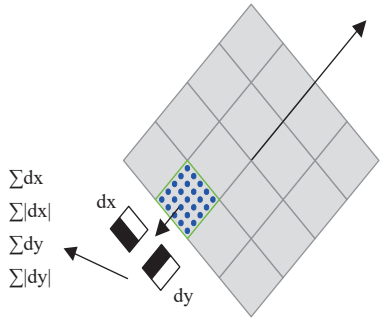

Figure 6 SURF feature point descriptors

2) ORB

The ORB algorithm[19] is a feature point extraction and description algorithm that combines the FAST algorithm[20] with the BRIEF algorithm[21]. It solves the problem of feature points lacking scale invariance by using the FAST algorithm to detect feature points at different levels of the pyramid. Additionally, the ORB algorithm assigns a dominant orientation to each feature point. This is done by computing the position of the intensity centroid within the neighborhood box of the feature point. The direction from the feature point to the intensity centroid determines the dominant orientation, ensuring that the feature descriptors have rotational invariance.

2.2.2 Feature point descriptors

1) SURF descriptor

The SURF descriptor is a 64-dimensional vector obtained by computing Haar wavelet features in 16 sub-regions within a square box of side length 20 s around the main orientation of the feature point.

2) ORB descriptor

Due to the lack of scale invariance and rotational invariance in the descriptors generated by the BRIEF algorithm, the ORB algorithm addresses these issues by constructing a spatial pyramid and assigning a main orientation to feature points. This effectively solves the problems in BRIEF and ultimately leads to the development of the ORB descriptor.

3) BRISK descriptor

The BRISK descriptor uses a uniform sampling pattern, as shown in Figure 7a (only the points on the first circle are displayed for clarity). By continuously changing the radius R of the surrounding circle of a key point and performing uniform sampling, a 512-bit descriptor is obtained. The Hamming distance is used to measure the similarity of the environmental information around two feature points based on their descriptors.

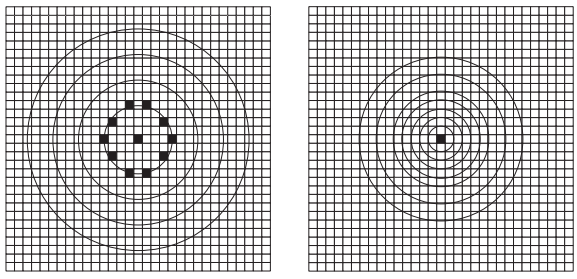

a. BRISK b. FREAK

Figure 7 Sampling pattern of the BRISK and FREAK descriptor

4) FREAK descriptor

FREAK is also a binary descriptor that can be applied to all key points detected by various algorithms such as SIFT, SURF, or ORB. However, in FREAK, the sampling density increases as the points get closer to the center. This means that the sampling points are denser on the circles closer to the key point, as shown in Figure 7b. The FREAK model consists of seven concentric circles centered around the key point.

2.3 Feature matching improvement

(1) This article selects the SURF algorithm to extract image feature points and uses the FREAK algorithm to describe the feature points. However, the extracted feature points tend to cluster together, resulting in uneven distribution and mainly concentrated in highly textured areas. The clustering leads to two main issues: The traditional SURF algorithm extracts feature points from the entire

image. However, during the matching phase, only the feature points that overlap between the reference and the stitched image are used. Consequently, feature points in non-overlapping regions not only prolong the matching process and reduce efficiency, but also elevate the risk of mismatching.

(2) The traditional SURF algorithm uses a brute force matcher to compare the feature descriptor vectors of the first image with all the feature descriptors of the second image. The pair with the highest similarity (i.e., the shortest distance between the two descriptors) is selected as the best match. However, this method often leads to a large number of incorrect matches due to the symmetric nature of image structures, resulting in low image registration accuracy.

To address problem (1), a grid-based feature detection method in overlapping region was proposed, as shown in Figure 8. Firstly, the extracted feature points from the image are divided into several equally sized grids. The grids in the overlapping region are extracted as the regions of interest. For each individual grid, the SURF algorithm is used to extract feature points, and the top n feature points with higher feature values are retained (shown as green feature points in Figure 8). Then, the image is divided into grids and feature extraction is performed. The feature points retained from each individual grid are aggregated to form a complete set of feature points for the entire image. Finally, the FREAK algorithm is used for feature description using binary descriptors.

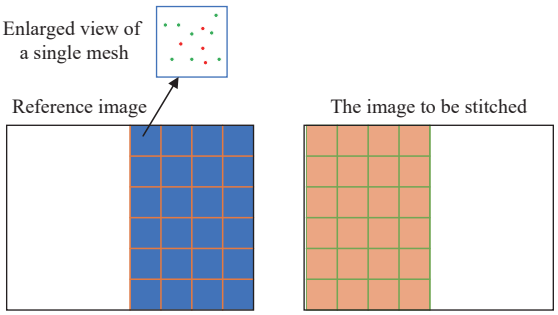

Figure 8 Schematic diagram of feature extraction in overlapping regions based on grid segmentation

To address problem (2), we employ a second screening-based image registration method to reduce the chances of incorrect matches and improve the accuracy of image registration. Firstly, a coarse filtering is performed on the matching points based on the Hamming distance. Then, the PROSAC algorithm[24] is used as a replacement for the RANSAC algorithm in the second filtering step to improve the accuracy of image matching.

The specific process of PROSAC is shown in Figure 9. This method can exclude matching items with large differences between descriptors during the filtering process, but a threshold needs to be set in advance. Since the difference between descriptors varies greatly for different images, this paper adopts an automatic threshold calculation method for filtering. Firstly, the Hamming distance of all matching point pairs is calculated, and the minimum distance of the key point pairs is obtained. Then, the Hamming distance of all matching points is compared with k times $d_{\min}$, and the matching items with a difference smaller than the threshold (i.e., k times $d_{\min}$) are retained. By introducing a threshold coefficient k, the problem of significantly different thresholds between different images is effectively solved, allowing the algorithm to select a reasonable threshold based on its own image characteristics combined with the threshold coefficient.

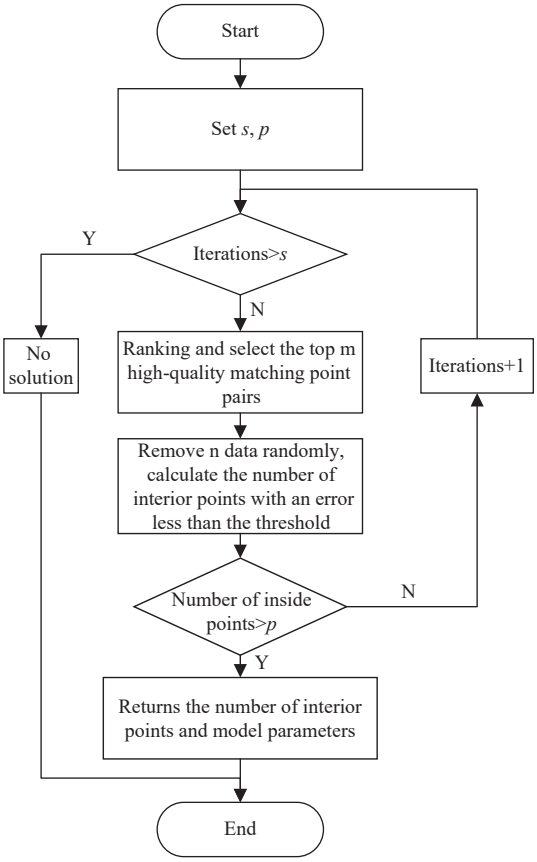

Figure 9 Flowchart of the PROSAC algorithm

2.4 Image transformation and image fusion

After two rounds of filtering, the misaligned point pairs in the matching point pairs are eliminated one by one, and only the optimal matching point pairs set, $f_a(x,y)$ and $f_b(x,y)$, are retained. The optimal homographic matrix $\boldsymbol{H}$ is then computed using the optimal matching point pairs set to perform a perspective transformation, mapping the two images onto the same coordinate system. The transformation process is shown in Equation (2):

$$\begin{bmatrix} x_b \\ y_b \\ 1 \end{bmatrix} = \boldsymbol{H} \begin{bmatrix} x_a \\ y_a \\ 1 \end{bmatrix} = \begin{bmatrix} h_0 & h_1 & h_2 \\ h_3 & h_4 & h_5 \\ 0 & 0 & 1 \end{bmatrix} \begin{bmatrix} x_a \\ y_a \\ 1 \end{bmatrix} \tag{2}$$

where, h_0, h_1, h_3, h_4 represents the rotational component of the perspective transformation, and h_2, h_5 represents the translational component of the perspective transformation.

In practical acquisition systems, the images stitched are captured by two cameras, and there are slight differences in camera parameters. The captured images also have subtle differences in grayscale and lighting conditions. After stitching, there are traces left at the stitching positions of the overall image, so it is necessary to process the stitching traces through image blending. A fusion algorithm is adopted to blend the images based on the optimal seam line[25]. It mainly calculates the intensity values and then uses dynamic programming to find the optimal path with the highest intensity values in the overlapping region, resulting in the best seam line. The Sobel operator is commonly used to calculate the structural difference intensity, as shown in Equation (3):

$$E_g(x,y) = (\boldsymbol{S}_x \times (I_1(x,y) - I_2(x,y)))^2 + (\boldsymbol{S}_y \times (I_1(x,y) - I_2(x,y)))^2 \tag{3}$$

where, $\boldsymbol{S}_x$ and $\boldsymbol{S}_y$ represent the horizontal and vertical direction Sobel operators.

Then, through the dynamic programming approach, the

scanning is performed from top to bottom. The starting point of the optimal seam line is set as the corresponding point in the first row of pixels. Then, the intensity values of the left, middle, and right points in the next row are calculated, and the point with the minimum intensity value is selected to continue the iteration until the last row. Finally, the line with the minimum intensity value is chosen as the optimal seam line for image fusion. The overall process of image stitching is shown in Figure 10.

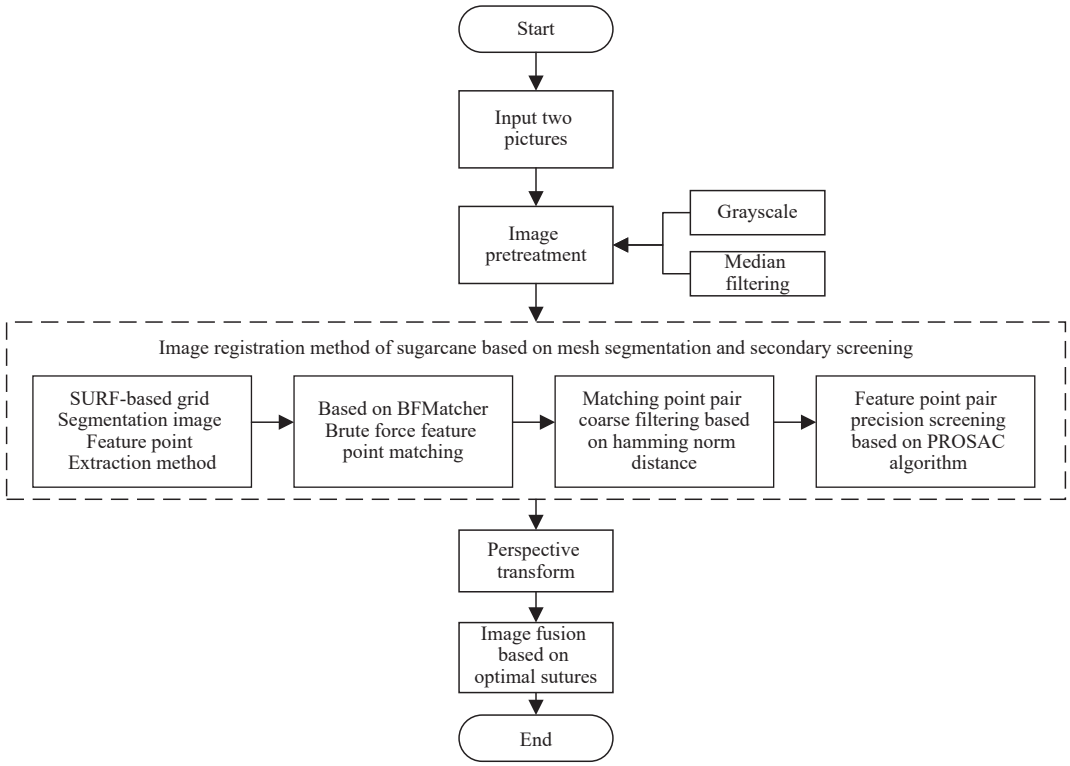

Figure 10 Horizontal transport-based sugarcane image stitching method

3 Experiment results and analysis

The experiments in this study were conducted on a PC machine with an Intel (CITM) i7-9750 CPU, 16 GB of RAM, running a 64-bit Windows 10 operating system. The programming software used was PyCharm, and the programming language used was Python.

To evaluate the speed of image stitching, we use the time taken for image stitching as the evaluation metric. Meanwhile, during the stitching process, the evaluation of the stitching quality is primarily based on visual observation, which is subjective and influenced by personal preferences. Therefore, this paper introduces the concept of image entropy[26] to analyze and evaluate the stitched images. Image entropy is commonly used to assess the quality of processed images and reflects the average amount of information in an image. It is calculated using Equation (4), where a higher entropy value indicates clearer texture details in the entire image.

$$IE = -\sum_{i=0}^{255} P(i)\log_2 P(i) \tag{4}$$

In the equation, $P(i)$ represents the probability of grayscale value i in the entire image.

3.1 Experiments for decision of window size

Three window sizes, namely 3×3, 5×5, and 7×7, are selected to perform median filtering on the sugarcane image contaminated with salt-and-pepper noise. The results are shown in Figure 11. It can be observed that when using a 5×5 or 7×7 window for filtering, the image becomes distorted due to the large window size. On the other hand, the 3×3 filter size can effectively remove salt-and-pepper noise while preserving image features. Therefore, this study adopts a 3×3 filter size for median filtering.

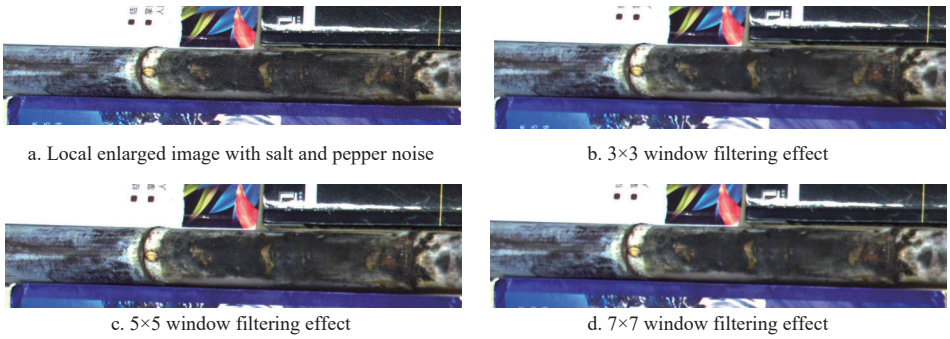

a. Local enlarged image with salt and pepper noise

b. 3×3 window filtering effect

c. 5×5 window filtering effect

d. 7×7 window filtering effect

Figure 11 Magnified view of the median filtering results with different window sizes

3.2 Experiments for feature point extraction algorithms and descriptors comparison

We conducted experiments by combining different feature point extraction and description methods to compare their performance on the collected images. From these experiments, we selected the best method as the baseline method. During the

matching process, fast nearest neighbor search was used for feature point filtering. Finally, the number of feature points extracted is compared based on the time required for feature extraction and matching, and the misalignment rate for different combinations of methods, and evaluated their performance.

From Table 1, it can be observed that the ORB feature extraction algorithm has the fastest speed but extracts fewer effective feature points, resulting in a higher misalignment rate. On the other hand, the SURF algorithm has a lower speed compared to ORB but offers higher accuracy. When the SURF feature extraction algorithm is combined with the FREAK descriptor, it retains more effective feature points, ensuring both registration accuracy and higher speed compared to the original algorithm. Therefore, the combination of SURF and FREAK algorithms is selected as the baseline method.

Table 1 Experimental data for comparing different feature point extraction algorithms

Combination	Hessian matrix threshold/ number of feature points	Coefficient *k*	Number of feature points before/after	Time consumed/ ms	Misalignment rate
SURF+SURF descriptor	2000	0.25	3132/66	4218	None
		0.35	3132/203	4328	None
		0.45	3132/365	4062	None
		0.55	3132/522	4422	Fewer
ORB+ORB descriptor	2000	0.25	2000/15	2125	None
		0.35	2000/75	1594	Fewer
		0.45	2000/186	2812	Few
		0.55	2000/318	1610	More
SURF+FREAK descriptor	2000	0.25	2719/83	2647	None
		0.35	2719/252	2812	None
		0.45	2719/405	2875	Fewer
		0.55	2719/549	2938	Few
SURF+BRISK descriptor	2000	0.25	2957/128	4735	None
		0.35	2957/274	4954	None
		0.45	2957/437	4610	Fewer
		0.55	2957/580	5156	Few
ORB+FREAK descriptor	2000	0.25	1520/14	1500	Fewer
		0.35	1520/61	1750	Much more
		0.45	1520/164	1766	Much
		0.55	1520/304	304	Much
ORB+BRISK descriptor	2000	0.25	1880/32	4156	Fewer
		0.35	1880/123	3750	Few
		0.45	1880/236	3641	Much
		0.55	1880/359	3641	Much

3.3 Experiment result of grid segmentation for feature extraction

After comparing different feature extraction algorithms, the SURF algorithm was selected for feature point extraction, combined with the FREAK algorithm for feature point description. The results of image feature extraction are shown in Figure 12, where the image is in grayscale and the feature points are represented in color. As shown in Figure 12, it can be observed that the extracted feature points are clustered and unevenly distributed, mainly concentrated in highly textured areas. Figure 13 shows the results of SURF feature point extraction based on grid segmentation.

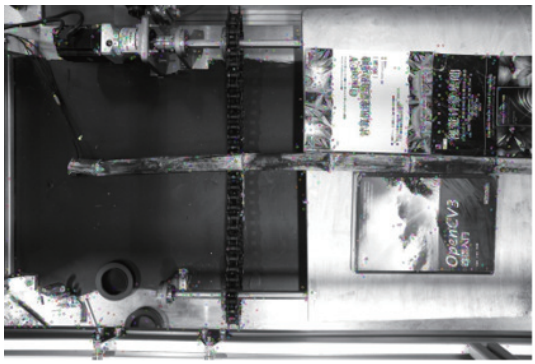

Figure 12 SURF

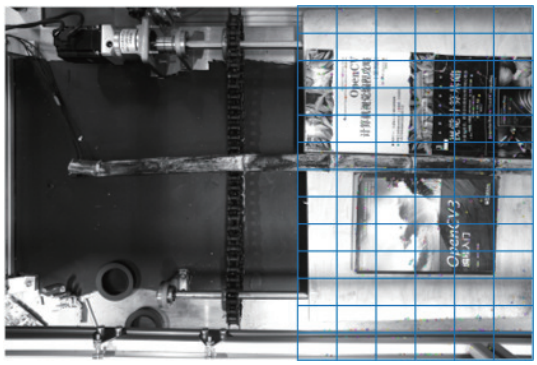

Figure 13 SURF and grid segmentation

3.4 Experiment result of image registration with secondary filtering

The traditional SURF algorithm uses brute-force matching, which generates many mismatched point pairs, as shown in Figure 14. To address this issue, a preliminary filtering step is performed by calculating the Hamming distance. This step helps eliminate a large number of mismatched point pairs, as shown in Figure 15. However, despite the preliminary filtering, some mismatched point pairs still remain. To further improve the matching results, the PROSAC algorithm is introduced. The final matching results are shown in Figure 16, demonstrating the effectiveness of the proposed secondary filtering image registration method in eliminating mismatched points during the stitching process.

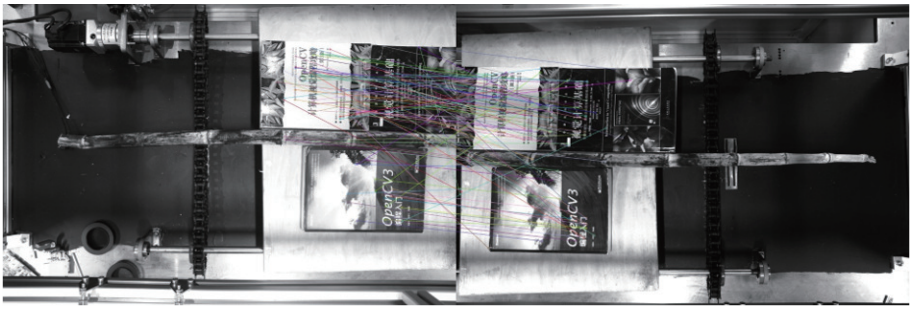

Figure 14 Brute-force matching results

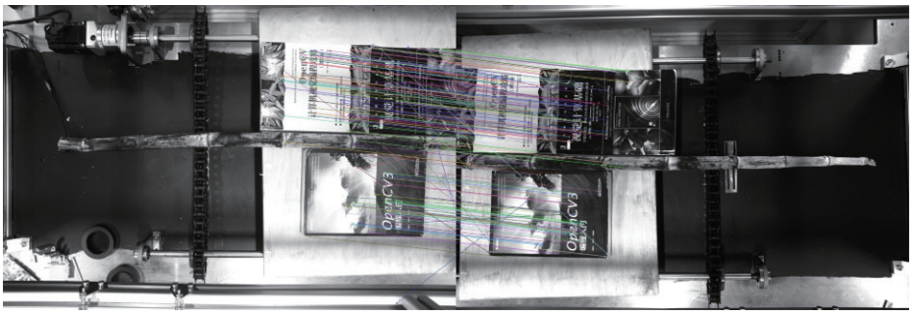

Figure 15 Matching results after preliminary filtering

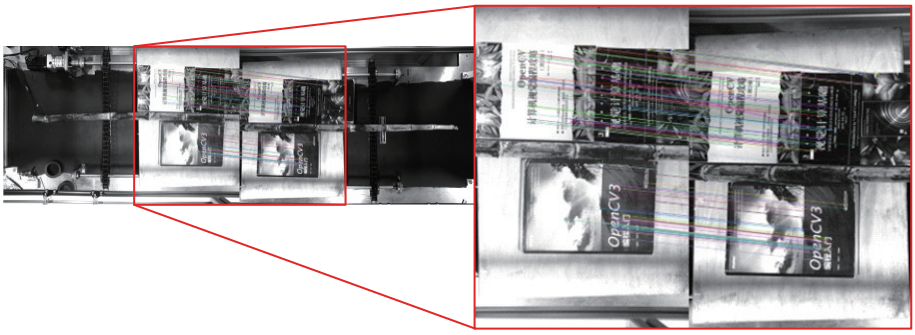

Figure 16 Final matching results

3.5 Experiment result of image transformation and image fusion

After two rounds of filtering, the mismatched point pairs in the matching results were eliminated one by one, leaving only the optimal set of matching point pairs, denoted as $f_a(x,y)$ and $f_b(x,y)$, between the two images. Using this optimal set of matching point pairs, a perspective transformation was applied to map the two images onto the same coordinate system.

Two fusion algorithms were then employed to merge the transformed images. A local region of the fused images was selected for comparison, as shown in Figure 17. From the highlighted region in Figure 17a, it can be observed that the image

a. Fade-in and fade-out fusion method b. Best seam line fusion method

Figure 17 Comparison of fusion results

Figure 18 Final stitched image

fused using the fade-in and fade-out fusion method exhibits ghosting artifacts. However, the image fused using the best seam line fusion method effectively resolves the ghosting issue. The final stitched image is shown in Figure 18, which demonstrates the successful fusion of the two images after the perspective transformation and the application of the optimal fusion algorithm.

3.6 Comparison of image stitching speed and quality

To validate the improvement in stitching speed achieved by our algorithm, we conducted a comparative experiment using randomly selected sets of 10 sugarcane images. The algorithms with the SURF algorithm and the ORB algorithm are compared as shown in Figure 19. As shown in Figure 19, it can be observed that the ORB algorithm has the shortest runtime, while our algorithm has a slightly longer runtime than the ORB algorithm, but is significantly lower than the SURF algorithm. This is because our algorithm focuses only on the repetitive regions for grid segmentation and feature extraction, reducing the overall processing time. Additionally, the PROSAC algorithm, used in our approach, eliminates ineffective iterations compared to the RANSAC algorithm, reducing the time required for the second filtering step. The overall average stitching time using our improved algorithm is reduced by 1314 ms compared to the unimproved SURF algorithm.

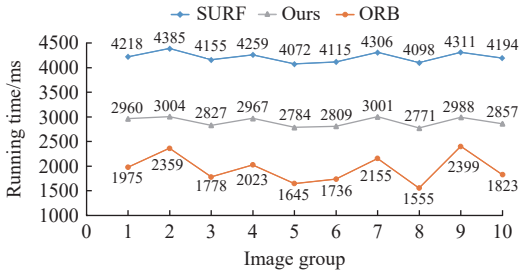

Figure 19 Speed comparison of different algorithms for image stitching

The final results of image stitching using different algorithms are shown in Table 2, and the computation of IE is given by Equation (4).

Table 2 Quality comparison of image stitching using different algorithms

Algorithm	IE	
	Group 1	Group 2
SURF	6.36	6.29
ORB	6.09	6.06
Ours	6.37	6.31

According to Table 2, it can be observed that the improved algorithm yields significantly higher image entropy compared to the ORB algorithm. Additionally, the overall stitching speed of the algorithm is reduced by 1314 ms compared to the traditional SURF algorithm, which is demonstrated effectively.

4 Conclusions

The excessive length of sugarcane poses a challenge in obtaining a comprehensive image of the entire cane during horizontal transportation, leading to reduced efficiency in cutting and planting operations. To address this issue, this paper proposes an improved image stitching algorithm based on the SURF algorithm. The main results are as follows:

1) The artificial markers are introduced to extract sufficient feature points for assisted matching, which can overcome the low matching accuracy due to the smooth surface of sugarcane.

2) The mainstream feature extraction algorithms and descriptors are introduced, and the SURF algorithm combined with FREAK is selected as the basic algorithm based on experimental results. Furthermore, to address the issue of slow image stitching caused by the need to extract global image feature points and the uneven distribution of feature points, this paper improves the SURF algorithm by using the idea of grid segmentation. Experimental results demonstrate that grid segmentation can significantly reduce useless feature points and improve the speed of feature matching.

3) A secondary screening-based image registration method is proposed to improve the issue of incorrect feature point matching. To address the problem of overlapping during stitching, the paper introduces the image fusion method using the best seam line and verifies its effectiveness through experiments. The experimental results show that the proposed algorithm achieves good results in terms of stitching speed and quality, enabling high-quality and wide-angle sugarcane image stitching.

Acknowledgements

This work was supported by the Natural Science Foundation of Hainan Province, China (Grant No. 323MS089 and 324MS095).

[References]

[1] Nare B, Tewari V K, Chandel A K, Kumar S P, Chethan C R. A mechatronically integrated autonomous seed material generation system for sugarcane: A crop of industrial significance. Industrial Crops and Products, 2019; 128: 1–12.

[2] Chen J Q, Qiang H, Xu G W, Wu J H, Liu X, Mo R X, et al. Sugarcane stem nodes based on the maximum value points of the vertical projection function. Ciencia Rural, 2020; 50(12): 1–10.

[3] Yang R, Li J, Liu Q, Huang W S, Yin K, Qiao X, et al. Gradient-based method for the identification of multi-nodes in sugarcane. Information Processing in Agriculture, 2020; 7(4): 491–499.

[4] Wang F K, Liu Q, Huang M Z, Qiao X, Huang Y Q. Research on sugarcane seed-bud location based on anisotropic scaling transformation. Applied Engineering in Agriculture, 2021; 37(6): 1119–1130.

[5] Chen W, Ju C W, Li Y Z, Hu S S, Qiao X. Sugarcane stem node recognition in field by deep learning combining data expansion. Applied Sciences-Basel, 2021; 11(18): 8663.

[6] Wang W W, Li C, Wang K, Tang L L, Ndiluau P F, et al. Sugarcane stem node detection and localization for cutting using deep learning. Frontiers in Plant Science, 2022; 13: 1089961.

[7] Wang Z B, Yang Z K. Review on image-stitching techniques. Multimedia Systems, 2020; 26(4): 413–430.

[8] Tang H B, Chao Y, Liu W H, Ma C X. Review of measurement methods for large-size parts based on machine vision. Electronic Measurement Technology, 2021; 44(17): 33–40.

[9] Wijiaya M C. Template matching using improved rotations Fourier transform method. International Journal of Electronics and Telecommunications, 2022; 68(4): 881–888.

[10] Li T C, Wang J L, Yao K N. Subpixel image registration algorithm based on pyramid phase correlation and upsampling. Proc. Signal Image and Video Processing, 2022; 16(7): 1973–1979.

[11] De Castro E, Morandi C. Registration of translated and rotated images using finite Fourier transforms. IEEE Transactions on pattern analysis and machine intelligence, 1987; 5: 700–703.

[12] Harris C, Stephens M. A combined corner and edge detector. Alvey vision conference, 1988; 15(50): 10–5244.

[13] Shan B Y, Zhu Z C, Zhang Y H, Qiu C B. A real-time SIFT algorithm for planetary surface feature extraction. Laser & Optoelectronics Progress, 2021; 58(2): 211–218.

[14] Anil B. Automatic image stitching using SURF and RANSAC based homography estimation. Journal of Polytechnic-Politeknik Dergisi, 2022; 25(2): 597–604.

[15] Lee K Y, Sim J Y. Warping residual based image stitching for large parallax. 2020 IEEE/CVF Conference on Computer Vision and Pattern

Recognition (CVPR). IEEE Computer Society, 2020; pp.8195–8203.
[16] Bouchekara H R E H, Sadiq B O, Zakariyya S, Sha'aban Y A, Sharhriar M S, Isah M M. SIFT-CNN pipeline in livestock management: A drone image stitching algorithm. Drones, 2022; 7(1): 17.
[17] Burian D, Kudera C, Pucher M, Merzdovnik G. Automated stitching of noisy scanning electron microscopy images for integrated circuit reverse engineering. 2022 IEEE Physical Assurance and Inspection of Electronics (PAINE). IEEE, 2022; 1–7.
[18] Chen J, Li Z X, Peng C L, Wang Y, Gong W P. UAV image stitching based on optimal seam and half-projective warp. Remote Sensing, 2022; 14(5): 1068.
[19] Subramanyam V, Kumar J, Singh S N. A hybrid descriptor for low-textural image stitching in real-time surface inspection systems. Multimedia Tools and Applications, 2023; 1–23.
[20] Li A H, Liu X S, Gong W, Sun W S, Sun J F. Prelocation image stitching method based on flexible and precise boresight adjustment using Risley prisms. Journal of the Optical Society of America A-Optics Image Science and Vision, 2019; 36(2): 305–311.
[21] Huang C W, Pan X, Cheng J C, Song J J. Deep image registration with depth-aware homography estimation. IEEE Signal Processing Letters, 2023; 30: 6–10.
[22] Zhou D Q, Zhao W B, Chen Y X, Zhang Q J, Deng G R, He F G. Identification and localisation algorithm for sugarcane stem nodes by combining YOLOv3 and traditional methods of computer vision. Sensors, 2022; 22(21): 8266.
[23] Azimbeik K, Mahdavi S H, Rofooei F R. Improved image-based, full-field structural displacement measurement using template matching and camera calibration methods. Measurement, 2023; 221: 112650.
[24] Chandra T B, Verma K. Analysis of quantum noise-reducing filters on chest X-ray images: A review. Measurement, 2020; 153: 107426.
[25] Lan Z L, Li Z, Li W. Lane image sequence stitching based on SURF and optimal seam. Journal of Chongqing JiaoTong University (Natural Science), 2019; 38(10): 13–18.
[26] Liu T C, Song Y S, Li J W, Zhao X. Improved algorithm for high-resolution image stitching based on ORB features. Laser & Optoelectronics Progress, 2021; 58(8): 85–92.